ACS OMEGA

Article

Cite This: ACS Omega 2019, 4, 8071−8080

http://pubs.acs.org/journal/acsodf

Amyloid-Based Injectable Hydrogel Derived from Hydrolyzed Hen Egg White Lysozyme

Lujuan Yang,[†] Haoyi Li,*[,†,‡] Linxia Yao,[†] Yang Yu,[†] and Gang Ma*[,†]

[†]Key Laboratory of Medicinal Chemistry and Molecular Diagnosis of Ministry of Education, Key Laboratory of Analytical Science and Technology of Hebei Province, College of Chemistry and Environmental Science, Hebei University, Baoding 071002, China

[‡]College of Chemistry and Materials Science, Langfang Teachers University, Langfang 065000, China

Supporting Information

ABSTRACT: Injectable hydrogels based on synthetic peptides have shown great promise in many biomedical applications. Yet, the high cost generally associated with synthetic peptides hinders the practical use of such peptide-based injectable hydrogel. To overcome this drawback, here, we propose to use the peptides from hydrolyzed low-cost natural protein as an economical and convenient peptide source to prepare an injectable hydrogel. We demonstrate the effectiveness of this alternative strategy using hen egg white lysozyme (HEWL) as an example. We used the peptide fragments from hydrolyzed HEWL as the gelator, and the magnesium ion as the performance enhancer to prepare the injectable hydrogel. We showed that the hydrogel is an amyloid gel as it was formed by a dense network of amyloid fibrils. We also showed that the hydrogel possesses a thixotropic property and displays a low cytotoxicity. The hydrolysis extent of HEWL was found to be a critical factor that influences the performance of the hydrogel. A fluorescence assay based on 8-anilinonaphthalene-1-sulfonic acid was proposed as a mean to precisely and conveniently control the hydrolysis extent of HEWL to enable the best injectability performance. At last, using doxorubicin as a model compound, we explored the potential of this amyloid-based hydrogel as an injectable drug carrier.

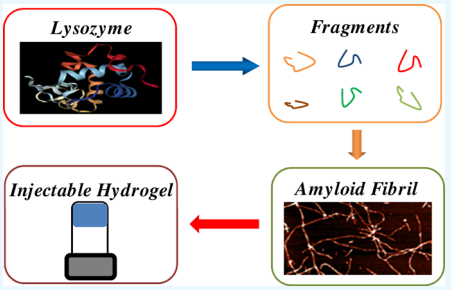

INTRODUCTION

Hydrogels are a class of soft materials that possess three-dimensional networks, which can entrap a large amount of water, while maintaining their structural integrity. Their easily tunable physical and chemical properties have made it possible for hydrogels to be employed in many modern engineering and technological areas.[1] In particular, hydrogels with biocompatibility and biodegradability are perfect candidates for biomedical applications including as scaffolds in tissue engineering,[2−11] as delivery vehicles for injectable therapeutics,[4,12−25] as coating for implantable biomedical devices,[26−28] and as bioadhesives in surgery.[29−32]

Injectable hydrogel is a unique type of hydrogel for biomedical applications. It can be easily applied to the target site through a syringe and then undergo a rapid in situ gelation through either chemical cross-linking or physical association. The injectable property makes such hydrogel possess some apparent advantages over noninjectable hydrogels. For example, when used as implantable materials, injectable hydrogels can readily assume the shape of the cavity, thus providing a perfect fit and contact between the hydrogel and tissue; when used in tissue engineering and drug delivery, cells and drug molecules can be easily incorporated into the hydrogel through simple mixing with the hydrogel before injection.[33,34] Injectable hydrogels can be formed by diverse types of chemical and biological systems, such as peptides and proteins, polymer blends, block copolymers, colloids, polyelectrolytes, host−guest complex, etc.[34] Among these systems, peptide-based hydrogels have attracted great attention in recent years due to their good biocompatibility and showed great promises in the biomedical fields.[35−47]

Despite these exciting progresses made by scientists in recent years, peptide-based injectable hydrogels still suffer from high cost. The peptides used in injectable hydrogels are usually synthetic peptides obtained through solid-phase synthesis. It is known that peptide synthesis can be very costly, in particular, with respect to long peptide synthesis. To overcome this drawback, some scientists have explored to construct an injectable hydrogel with ultrashort peptides or conjugated single amino acid.[42,47−53] For example, Mahler et al. discovered that an Fmoc-modified dipeptide, Fmoc-diphenylalanine peptide, could easily form an injectable hydrogel when prepared at a high concentration in aqueous solution.[48] Such hydrogel was stable under a variety of conditions including a broad range of temperatures, wide pH range, and even under some harsh conditions such as in the presence of denaturants and strong acid. These excellent conditions render this dipeptide-based injectable hydrogel a wide range of potential applications.[48] Baral et al. developed a synthetic tripeptide-based hydrogel.[42] The tripeptide consists of 11-amino-

Received: December 13, 2018
Accepted: April 24, 2019
Published: May 2, 2019

DOI: 10.1021/acsomega.8b03492
ACS Omega 2019, 4, 8071−8080

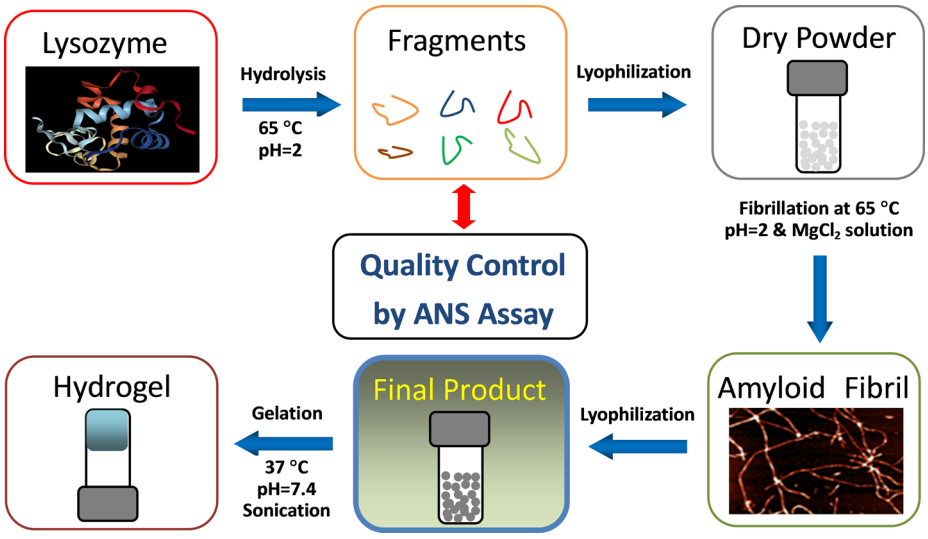

Figure 1. Strategy of making an injectable hydrogel from hydrolyzed HEWL.

undecanoic acid and Phe-Phe residues. The hydrogel by such tripeptide exhibits excellent thixotropic property and injectability. The hydrogel were used as a delivery vehicle for the sustained release of an antibiotic vancomycin and vitamin B12.[42] Thota et al. designed a conformationally restricted dipeptide, LeuΔPhe, containing an α,β-dehydrophenylalanine residue.[47] This gelator can form a highly stable and mechanically strong hydrogel under mild physiological aqueous conditions and shows excellent biocompatibility and injectability. Controlled release of several hydrophobic and hydrophilic drug molecules with this novel hydrogel has been demonstrated. The hydrogel was further used to entrap an antineoplastic drug to treat tumor in a mouse model.[47] Besides developing low-cost synthetic ultrashort peptides, we believe that looking for peptides from low-cost natural sources could be an alternative way to construct a peptide-based injectable hydrogel. To this end, we herein propose to use peptides from hydrolyzed low-cost natural protein such as hen egg white lysozyme (HEWL) as an economical and convenient peptide source to prepare an injectable hydrogel. Using the peptide fragments from hydrolyzed HEWL as the gelator, and the magnesium ion as the performance enhancer, we are able to prepare an injectable amyloid gel. Factors that influence the injectability of the hydrogel are investigated, and the hydrolysis extent of HEWL was found to be the most influential. A fluorescence assay based on 8-anilinonaphthalene-1-sulfonic acid (ANS) was proposed as a mean to precisely and conveniently control the hydrolysis extent of HEWL to enable the best injectability performance. At last, using doxorubicin as a model compound, we explored the potential of this amyloid-based hydrogel as an injectable drug carrier.

RESULTS AND DISCUSSION

The aim of our study is to develop a low-cost injectable peptide-based hydrogel system. In previous reported injectable hydrogels by synthetic peptides, it is very common to see that a hydrogel is composed of a dense network of nanofibrils by the designed peptides. This phenomenon inspired us to search for some amyloid fibril systems by some low-cost proteins to fulfill our goal. Amyloid fibril is a unique type of protein and peptide aggregate with fibrillar microscopic morphology.[54,55] The length of amyloid fibril can reach several microns, and the width of amyloid fibril is in nanoscale. So, amyloid fibrils are protein- and peptide-based nanofibrils. In vivo amyloid fibril formation can be a devastating event and about 40 human diseases are closely linked to the fibrillation of a particular protein or peptide.[54] Despite its pathological significance, amyloid fibril is now being considered as a promising building block for novel nanomaterials and has shown promises in a variety of applications such as sensing, tissue engineering, and drug delivery.[56−64] In recent years, we have been working with the amyloid system by hen egg white lysozyme (HEWL).[65−67] HEWL is a very low-cost natural protein and finds many applications in the food industry and pharmaceutics.[68] It is also a widely used model system in the amyloid research. When working with the HEWL amyloid system, we occasionally found that the amyloid incubation solution by hydrolyzed HEWL can form a hydrogel with some degree of thixotropic property. Namely, when we shake the gel-like incubation solution, it can turn from a solid gel to vicious liquid; after some resting time, it turned back to a solid gel. As the hydrogel system with thixotropic property can be a good candidate for an injectable hydrogel, our occasional discovery tells us that we might be able to develop an injectable hydrogel system based on the hydrolyzed HEWL system through some optimizations. In Figure 1, we show the general strategy of using HEWL to construct an injectable hydrogel with low cost and with ease. The first step is to hydrolyze HEWL under heat and acidic conditions. This is to generate a large amount of some highly amyloidogenic peptide fragments through selective hydrolysis at the sites of aspartic acid residue. These fragments are then lyophilized to give a dry powder. The obtained peptide powder is used to make the incubation solution with suitable concentration for amyloid fibrillation. The incubation solution also contains HCl and Mg^{2+}. HCl is to be used to provide an acidic environment, and the divalent Mg^{2+} ion is used to accelerate the amyloid formation and enhance the gelation performance. After amyloid fibrillation, the incubation solution is lyophilized again. This step gives the final product, namely, the precursor material for hydrogel. The final product is a mixture of amyloid fibrils, free peptides (i.e., the non-amyloidogenic peptides), and $MgCl_2$. It is ready to be used for making the injectable hydrogel. To make the injectable hydrogel, the amyloid fibril-containing powder is re-suspended

DOI: 10.1021/acsomega.8b03492
ACS Omega 2019, 4, 8071−8080

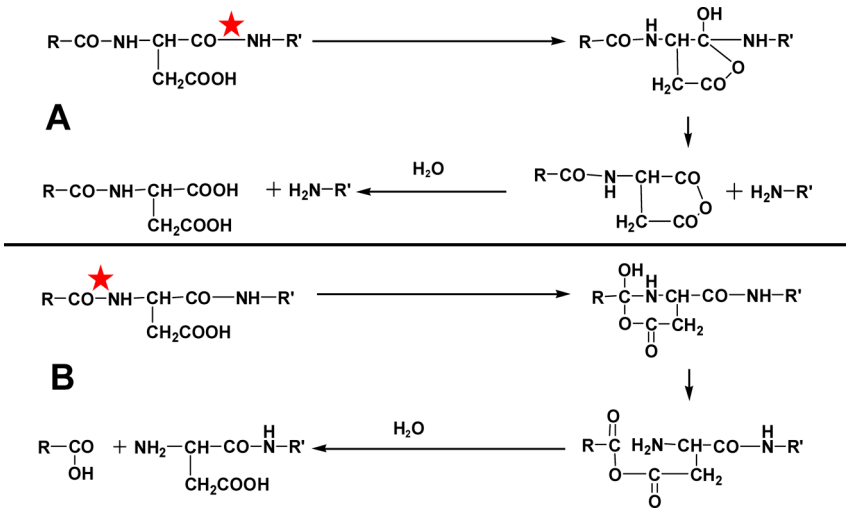

Figure 2. Hydrolysis mechanism of HEWL. (A) C-terminally partial hydrolysis of the peptide bond at the aspartic acid site (Asp-X type hydrolysis). (B) N-terminally partial hydrolysis of the peptide bond at the aspartic acid site (X-Asp type hydrolysis). Red star denotes the peptide bond to be cleaved.

in PB buffer. Moreover, the PB buffer can contain drugs for drug delivery purpose. After a brief sonication process with an ultrasonication bath, the suspension becomes a clear colloidal solution. The colloidal solution is ready to be used for syringe injection. In vitro testing at 37 °C shows that such colloidal solution (either with or without drug) can form gel rapidly, demonstrating its injectability. In addition, this hydrogel manufacturing process also includes a quality control step. In the following, we will provide detailed characterizations and descriptions for each step in Figure 1.

Hydrolysis of HEWL. Under acidic condition (i.e., pH = 2 or below), HWEL undergoes partial hydrolysis at the aspartic acid (Asp) site.[69−71] The partial hydrolysis mechanism is shown in Figure 2. The hydrolysis can occur on either the Asp-X peptide bond (referred to as Asp-X type hydrolysis in this work) or the X-Asp peptide bond (referred to as X-Asp type hydrolysis in this work). HEWL has seven aspartic acid residues as shown in its sequence in Figure 3. In principle,

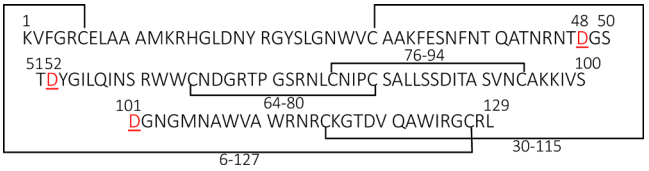

Figure 3. Amino acid sequence of HEWL.

partial hydrolysis of HEWL could generate a rather complex mixture of peptide fragments. Yet, in practice, previous studies have showed that HEWL cleaves mainly at the sites of D48, D52, and D101 through Asp-X type hydrolysis, thus generating the 49−101, 53−101, and 1−48/102−129 fragments.[70,71] The three important aspartic acid sites have been denoted in red color in Figure 3. The 49−101 and 53−101 fragments contain the disulfide bridges by Cys64−Cys80 and Cys76−Cys94, respectively; the 1−48/102−129 fragment contains the disulfide bridges by Cys6−Cys127 and Cys30−Cys115. The 49−101 and 53−101 fragments are highly amyloidogenic and are responsible for the amyloid formation of hydrolyzed HEWL. Figure S1 shows the Maldi-TOF MS results of the hydrolyzed HEWL in this study. The dominant MS peaks in the MS graph around m/z = 5318 and m/z = 5678 originate from the 49−101 and 53−101 fragments and their succinimide derivatives, respectively. The 1−48/102−129 fragment peak, which is around m/z = 8619, is not very intense in the MS graph likely due to its low Maldi-TOF response.

Amyloid Nature Characterizations. The obtained peptide fragments were used to make the incubation solution with suitable concentration for amyloid fibrillation. The pH of the incubation solution was adjusted to be 2 with aqueous HCl, and $MgCl_2$ was included in the incubation solution to accelerate the amyloid formation and enhance the gelation performance. The obtained fibrils were characterized using ThT fluorescent assay, AFM, Congo red (CR) assay, and FTIR spectroscopy to confirm its amyloid nature. The AFM characterization was presented in Figure 4A, which shows the formation of fibril-like peptide aggregates. These fibrils have average heights of 3 nm. In Figure 4B, the ThT fluorescent assay result shows the fluorescent enhancement around 480 nm under the excitation of 450 nm. ThT is a dye commonly used in the diagnostics of amyloid fibrils. Its fluorescent enhancement at 480 nm is the typical feature of ThT-stained amyloid fibrils.[72] In Figure 4C, the CR assay result reveals an absorption increase at about 540 nm after the CR binding onto the obtained peptide fibrils. CR is another commonly used dye in the diagnostics of amyloid fibrils. The appearance of 540 nm absorption of CR could indicate the presence of amyloid structure.[73] Figure 4D presents the FTIR characterization of the obtained peptide fibrils. The FTIR spectrum of HEWL fibrils features a prominent absorption at 1628 cm^{-1}, indicting the formation of β-sheet structure. The basic unit of an amyloid structure consists of two longitudinally extending β-sheets with their side chains forming a steric-zipper-like self-complementary intersheet structure. So, the presence of β-sheet secondary structure is an important feature of amyloid structure.[54,55,65,66,74] Overall, these AFM and spectroscopic characterizations confirm the formation of amyloid structure by the peptide fragments from hydrolyzed HEWL. The incubation solution containing the prepared amyloid fibrils are then lyophilized to get an amyloid fibril powder. The powder sample will be the final product (i.e.,

DOI: 10.1021/acsomega.8b03492
ACS Omega 2019, 4, 8071−8080

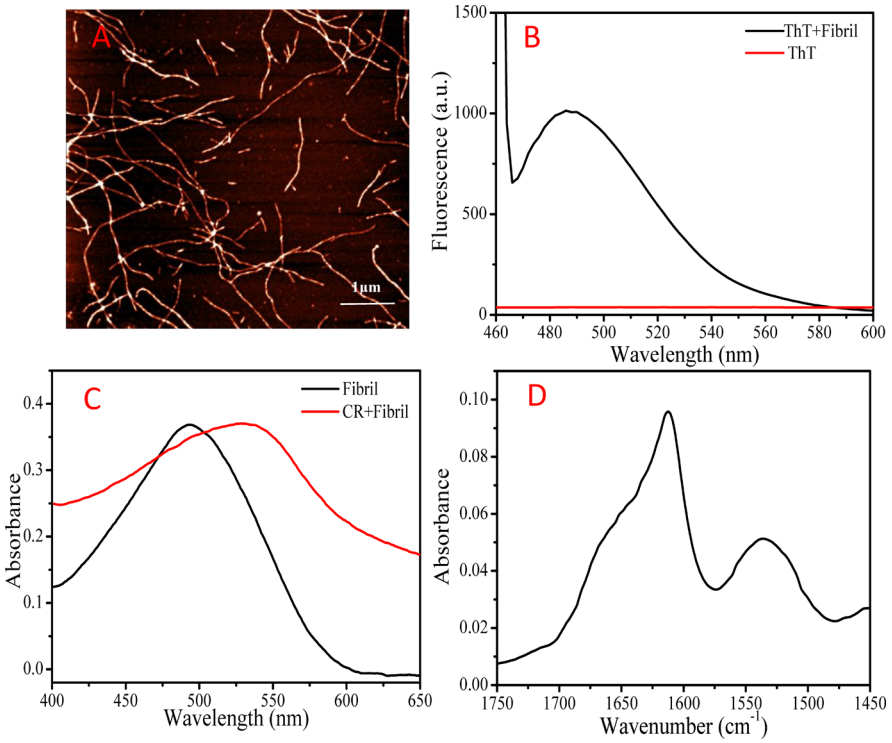

Figure 4. (A) AFM characterization of HEWL fibril; (B) ThT fluorescent assay; (C) CR assay; and (D) FTIR characterization of HEWL fibril. a.u.: arbitrary unit.

precursor materials) used for our quick and easy preparation of injectable hydrogel.

The final product is a mixture containing three major species: amyloid fibrils, nonamyloidogenic peptide fragments, and magnesium salt. The amyloid fibrils are formed by these amyloidogenic peptides derived from HEWL hydrolysis, namely, the 49−101 and 53−101 fragments and their derivatives. Some peptide fragments derived from HEWL hydrolysis such as the 1−48/102−129 fragment are non-amyloidogenic, and they are remained in the final product in the nonamyloid fibril form. As we can see, the final product is a rather complex mixture.

Injectable Hydrogel Preparation and TEM, SEM, XRD, and Rheological Characterizations. The lyophilized amyloid fibrils were dissolved into PB buffer at pH = 7.4. After sonication, the fibril and buffer mixture becomes a clear liquid suspension as shown in Figure 5A. Sonication step is helpful to better disperse the fibrils in the suspension. Such suspension is ready to be used as the injectable hydrogel. As shown in Figure 5A, the liquid suspension can become a solid gel within 5 to 10 min when incubated at 37 °C. Figure 5B shows how the injectable hydrogel with entrapped drug can be easily prepared. By simply mixing lyophilized amyloid fibril, drug (the anticancer drug, doxorubicin (Dox), is used here as an example) and PB buffer together and subject the mixture to sonication, we can obtain the injectable hydrogel with drug. The injectable hydrogel can be pulled out of the vial with a syringe right after the sonication step. The injected suspension can become a solid gel within 5 to 10 min when incubated at 37 °C.

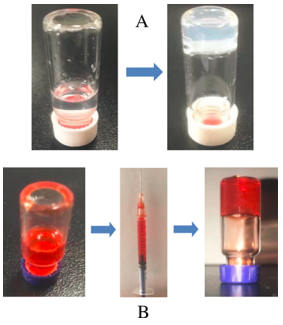

Figure 5. (A) Gelation of the amyloid fibril powder derived from hydrolyzed HEWL. (B) Injectability of the hydrogel with drug entrapment.

The hydrogel was characterized by TEM, SEM, and XRD, and the results were included in the Supporting Information. In Figure S2, the TEM image shows the presence of fibrillar aggregates in the hydrogel. The width of the fibril by TEM is about 18 nm. In Figure S3, the SEM image of the lyophilized hydrogel powder is shown. In Figure S4, the XRD analysis of the lyophilized hydrogel powder is shown. The XRD profile displays a sharp band at ∼4.7 Å and a broad band at ∼8 Å. The two bands correspond to the interstrand spacing and the intersheet spacing of the cross-β structure in the amyloid fibril, respectively.

We found that the above-prepared hydrogel possesses a thixotropic property. With current protocol, the hydrogel after vigorously shaking can become liquid suspension; the liquid suspension can then become gel again after 5−10 min resting time at 37 °C as demonstrated in Figure S5 in the Supporting Information. Thixotropic hydrogel is a mechano-responsive gel, which turns from "solid-like" gel state to "liquid-like" sol state through mechanical shaking, and returns to its original gel state upon the removal of external stress. This property allows us to easily maintain the fluid state of the prepared hydrogel through simple vortex or shaking before we transfer the

DOI: 10.1021/acsomega.8b03492
ACS Omega 2019, 4, 8071−8080

hydrogel into the syringe. This means that if for some reason, we need to wait for more time before using the syringe pulling the liquid suspension out of the vial, we can always let the suspension be subjected to vortex or shaking for a short duration of time to break any preformed gel in the vial during the waiting time. Therefore, the thixotropic property further eases the practical use of our injectable hydrogel.

The rheological properties of the injectable hydrogel were further characterized with a frequency sweep analysis and a step-strain time-dependent analysis. The results were presented in Figures 6 and 7. The frequency sweep results in Figure 6

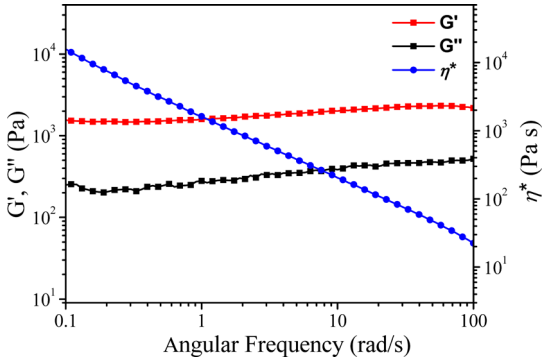

Figure 6. Frequency sweep rheological analysis of the hydrogel with 3% (w/v) (i.e., 30 mg/mL) HEWL concentration at a constant strain of 0.1%.

give the storage modulus (G′) and loss modulus (G″). Figure 6 was taken on the hydrogel prepared according to Figure 1. These measurements were carried out as a function of angular frequency by keeping a strain constant at 0.1%. The storage modulus for our hydrogel is in the order of 10^3. This value is similar to some reported self-assembling peptide hydrogels.[75,76] The storage modulus (G′) and the loss modulus (G″) represent the elastic portion and the viscous portion of the viscoelastic behavior of the sample, respectively. Intuitively, G′ describes the solid-state behavior of the sample, while G″ describes the liquid-state behavior of the sample. A solid-state sample such as a gel will have its G′ > G″, and a liquid sample such as a sol will have its G′ < G″. In Figure 6, we have G′ > G″. This indicates the formation of a solid state, that is, a gel. In the step-strain time-dependent rheological analysis in Figure 7, we varied the strain experienced by the hydrogel to see how the relationship of G′ and G″ change with strain and time. We

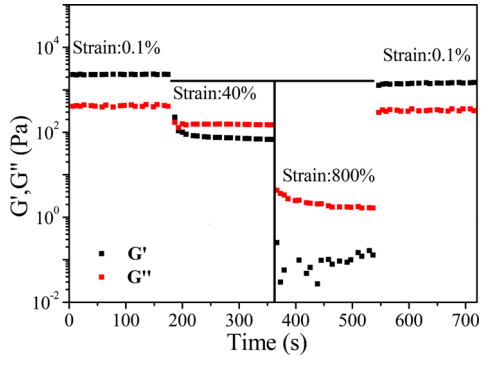

Figure 7. Step-strain time-dependent rheological analysis of the hydrogel with 3% (w/v) HEWL concentration with a fixed angular frequency of 3 rad/s.

performed this analysis with a procedure similar to the one use in previous work by Baral et al.[42] We first kept the hydrogel under a low constant strain of 0.1% for the first 200 s, and then the gel was suddenly subjected to a higher strain of 40%, and this strain was maintained for about 150 s. As shown in Figure 7, with 40% strain, we had G′ < G″, suggesting the disruption of the hydrogel and the formation of a sol. After about 150 s, the strain was suddenly further increased to a constant strain of 800% and was then maintained for another 200 s. As shown in Figure 7, we still had G′ < G″ during this operation. After this step, the strain was suddenly decreased to a constant strain of 0.1%, and we had an almost instantaneous recovery for G′ and G″. The step-strain time-dependent experiments thus demonstrate the good thixotropic property of our hydrogel. In the Supporting Information, we have included additional tests to further support our argument. These tests include two step-strain time-dependent experiments involving 100% strain (Figure S6) and 200% strain (Figure S7) and one strain sweep experiment result (Figure S8). Figure S9 shows the bar graph of selected points in Figure S8 and Table S1 presented the corresponding data.

Cytotoxicity of the Injectable Hydrogel. To examine the cytotoxicity of the hydrogel, we have performed a cytotoxicity study of the gel using L929 cell as a model system. The CCK-8 assay was employed to quantify the cell viability. As shown in Figure 8, the hydrogel shows a low

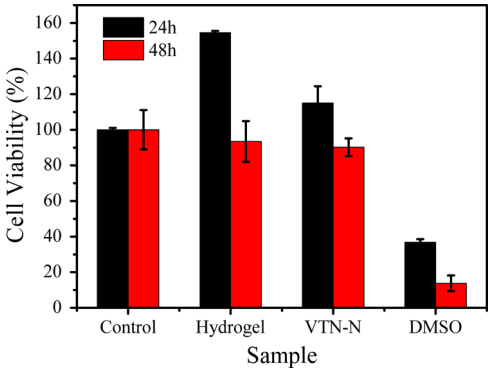

Figure 8. Cell viability of L929 cells after 24 and 48 h incubations with gel extracts.

cytotoxicity as compared with the negative (the "control" columns) and positive controls (the "DMSO" columns). In addition, the low cytotoxicity of the hydrogel is comparable to a commercial cell culturing product, VTN-N, which is used in stem cell research.

Drug Release from Hydrogel. The three dimensional structure of the hydrogel provide an excellent cage-like environment for the entrapment of small molecular drug. Moreover, the injectability of the hydrogel significantly eases the loading of drug into the hydrogel. In the following, we will use doxorubicin as a model compound to show the potential of the as-prepared hydrogel as a drug carrier. Dox is a chemotherapy medication commonly used to treat the cancers of the bladder, breast, stomach, lung, ovaries, thyroid, and others, as well as leukemia and Hodgkin's lymphoma. We now show that drug loading with 100% capacity can be achieved with a simple mixing step with our hydrogel system. We dissolved 30 mg of amyloid fibril powder into 0.5 mL of PB buffer to make a fibril suspension and dissolved a known amount of Dox (i.e., 0.2 mg, 0.4 mg, and 0.8 mg) into 0.5 mL

DOI: 10.1021/acsomega.8b03492
ACS Omega 2019, 4, 8071−8080

of PB buffer to make a drug solution. The suspension and drug solution were mixed together and then subjected to sonication. The obtained clear suspension with drug loading is the injectable hydrogel ready to use. With such protocol, 100% loading capacity could be achieved. In the following, we further performed an in vitro drug release test of the hydrogel loaded with Dox. One milliliter of the above injectable hydrogel loaded with Dox was put into a glass vial and incubated at 37 °C. Gelation occurred rapidly within 5−10 min. One milliliter of PB buffer was added on the surface of the hydrogel. Dox released from the hydrogel will diffuse into the PB buffer layer. At selected time points, 0.5 mL of PB buffer was sucked out by a pipette and then a fresh 0.5 mL of PB buffer was added into the glass vial to maintain a constant volume of PB buffer. The Dox concentration in the withdrawn solution was measured with UV−vis spectroscopy at 490 nm, which is a characteristic absorption band of Dox and is away from the peptide absorption, as shown in Figure S10. The cumulative release curves of the loaded Dox at three different concentrations are shown in Figure 9. The three curves showed similar release

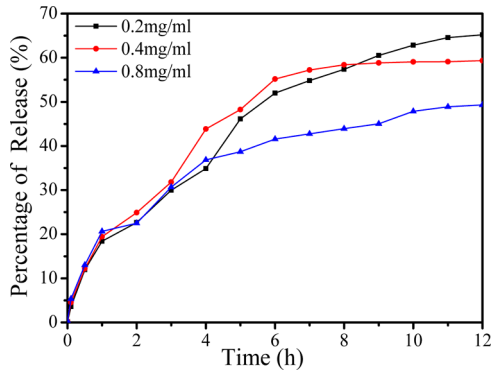

Figure 9. Cumulative percentage release plot of different concentrations of Dox entrapped in the hydrogel in PB buffer with pH = 7.4 at 37 °C.

profiles: the drugs released gradually over a period of 12 h. At the three concentrations, the accumulating released percentages of Dox in the drug-loaded hydrogels can all reach ∼50% or above. We also found that after a longer period of time (e.g., about 130 h), the drug-loaded hydrogel began to lose its integrity and diffused into the PB buffer.

ANS Assay as a Quality Control Approach. Reproducible hydrogel performance is critically important if the proposed hydrogel can eventually be commercialized or go to clinics. Therefore, a quality control step is an indispensable step during hydrogel production, as we have indicated in Figure 1. As for the protocols of making the injectable hydrogels, we have tested numerous combinations of several important factors that influence the hydrogel performance, including protein concentration, hydrolysis extent (or hydrolysis time), Mg^{2+} ion concentration, and amyloid fibril incubation time. The current protocol gives the hydrogel performance desired for this work. Namely, gelation can occur in a short time (i.e., 5 to 10 min), and hydrogel possesses a good thixotropic property. Among these factors, we found that the hydrolysis extent is a very influential factor that needs to be properly controlled. By adjusting the hydrolysis extent, we can adjust the gelation time and the drug release rate. For example, a shorter hydrolysis time can lead to a very long gelation time; a longer hydrolysis time can lead to a very slow drug release. However, we also found that the hydrolysis extent of the protein cannot be simply controlled by controlling an accurate hydrolysis time. Even we keep the hydrolysis time constant, the hydrolysis extent may vary to some extent from batch to batch. It is thus desired to have a better way to monitor the hydrolysis extent. We propose to use an ANS assay to monitor the hydrolysis extent. ANS is a widely used fluorescent probe in the field of protein science, and its fluorescence increases as it binds to hydrophobic residues of a protein.[77,78] When HWEL is hydrolyzed, the hydrophobic residues buried within HEWL interior will be exposed. With the progress of hydrolysis, more hydrophobic residues will be exposed. Because the fluorescence response of ANS is very sensitive to the presence of exposed hydrophobic residues, it can be used as an indicator for the hydrolysis extent. Figure 10 shows the ANS

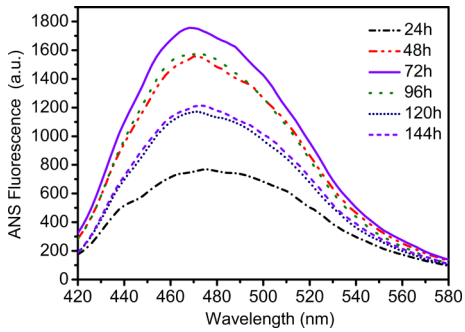

Figure 10. ANS assay during the hydrolysis of HEWL.

fluorescence change over time during hydrolysis. As we can see, ANS increases its fluorescence intensity over time (refer to the curves corresponding to 24 and 48 h) and then decreased (refer to the curves corresponding to 96, 120, and 144 h). ANS intensity reaches the highest (about 1800) at 72 h. We found when the ANS intensity reaches in between 1800 and 2000, the as-prepared hydrogel showed the desired performance in this work. ANS assay thus can be a convenient quality control step for a reproducible hydrogel performance during production.

Hypothesis on the Formation Mechanism of Amyloid-Based Hydrogel. The formation of a self-assembled hydrogel requires various noncovalent interactions during gelation.[79] These noncovalent interactions include hydrogen bonding, $\pi-\pi$ stacking, electrostatic, hydrophobic, and van der Waals interactions.[79,80] The lysozyme amyloid fibrils used to form the hydrogel in this work possess two properties, which could facilitate the establishment of these different types of noncovalent interactions during gelation. First, lysozyme consists of diverse types of amino acid residues such as aromatic residues, basic residues, and hydrophobic residues. The side chains of these residues could be utilized during the formation of these noncovalent interactions. Second, the amyloid fibril formed by a longer peptide or a protein (such as the lysozyme amyloid fibril here) usually has a "millipede-like" morphology.[81,82] Namely, the amyloid fibril looks like a millipede with a compact β-sheet central region being the main "body" and disordered peripheral regions being the short "legs". The residues in the disordered regions of the amyloid fibril can easily change their spatial orientations due to their flexible nature and help amyloid fibrils to establish noncovalent interactions with each other during gelation. In addition, Mg^{2+}

DOI: 10.1021/acsomega.8b03492
ACS Omega 2019, 4, 8071−8080

ions and the other nonamyloidogenic peptides should also play some roles in the establishment of noncovalent interactions.

CONCLUSIONS

In this work, we have demonstrated that an injectable peptide-based hydrogel can be easily prepared from a very low-cost natural protein, hen egg white lysozyme. The hydrogel utilizes the peptide fragments from hydrolyzed HEWL as the gelator, and the magnesium ion as the performance enhancer and is composed of a dense network of amyloid fibrils. The hydrogel possesses a thixotropic property and displays a low cytotoxicity. A fluorescence assay based on the dye of ANS was proposed as a convenient approach for quality control for a reproducible hydrogel performance. Using doxorubicin as a model compound, we explored the potential of this hydrogel as an injectable drug carrier.

EXPERIMENTAL SECTION

Materials. Hen egg white lysozyme (HEWL) (L6876) was purchased from Sigma-Aldrich (Saint Louis, USA). Thioflavin T (ThT) of ultrapure grade was purchased from AnaSpec (Fremont, USA). Congo red (CR) with >85% purity was purchased from Sigma-Aldrich (Saint Louis, USA). Potassium phosphate dibasic with >99% purity, potassium phosphate monobasic with >99% purity, and magnesium chloride ($MgCl_2$) with 99% purity were purchased from Aladdin (Shanghai, China). 8-Anilinonaphthalene-1-sulfonic acid (ANS) with 95% purity was purchased from TCI (Tokyo, Japan). Doxorubicin hydrochloride with 99% purity was purchased from a local vendor. Deionized water with a resistivity of 18.2 MΩ·cm was obtained from a Millipore system (Billerica, USA).

Injectable Hydrogel Preparation. The injectable hydrogel was prepared through the following protocols: (1) HEWL was dissolved in (pH = 2) aqueous solution at a concentration of 30 mg/mL. The solution was filtered through a 0.22 μm filter. The filtered solution was transferred into a glass vial and heated at 65 °C for about 3 days. During the incubation, hydrolysis of HEWL occurred, which generated peptide fragments. The exact stopping time point of the hydrolysis incubation was determined using an ANS assay that will be discussed later. The incubation solution containing peptide fragments was lyophilized to get a dried peptide powder. (2) The peptide powder was dissolved into (pH = 2) an HCl solution at a 30 mg/mL concentration, and 200 mM $MgCl_2$ was added into the peptide solution. The mixture solution was incubated at 65 °C for 5 days. This incubation process will generate peptide amyloid fibrils. The incubation solution was lyophilized to get a peptide fibril powder. This powder will be the precursor materials to make injectable hydrogel. (3) To make injectable hydrogel for practical use, we can simply mix the peptide fibril powder with pH = 7.3 PB buffer at a concentration of 30 mg/mL. The mixture is then subjected to ultrasonication for 20 min. The mixture is initially a liquid suspension and is suitable to be used as an injectable hydrogel. The liquid suspension will be solidified to become hydrogel in 5−10 min when incubated at 37 °C. To encapsulate drugs within the hydrogel, the drug can be added into the hydrogel by mixing the liquid suspension with drug solution.

Matrix-Assisted Laser Desorption/Ionization Time-of-Flight Mass Spectrometry (MALDI-TOF MS) Analysis. MALDI-TOF MS experiments were performed by a Bruker Ultraextreme MALDI-TOF/TOF mass spectrometer (Bremen, Germany). α-Cyano-4-hydroxycinnamic acid (CHCA) was chosen as the matrix for peptide MS analysis. The matrix was dissolved in 1:1 H_2O−acetonitrile solution with 0.1% TFA at a concentration of 5 mg/mL; the hydrolyzed HEWL powder was dissolved in water with 0.1% TFA at a concentration of 2 mg/mL. The two solutions were mixed together with 1:1 volume ratio (i.e., 1 μL:1 μL) and dropped onto the MALDI plate. The air-dried spot was subjected for MS analysis with an ion source voltage of 20 kV, a laser repetition frequency of 2000, and in a positive-ion linear mode. Each point was collected using 1000 laser shots. Data acquisition and analysis were performed with Bruker FlexControl 3.4 and FlexAnalysis 3.4 software. The instrument was calibrated with protein calibration standards with a molecular weight from 5000 to 20,000 Da before MS measurement.

AFM Measurement. All AFM images were taken on dried samples on mica in air with a NT-MDT Solver P47 scanning probe microscope (Zelenograd, Russia) using tapping mode. A 100 μm × 100 μm scanner was used throughout the AFM experiment. The cantilever from NT-MDT has a resonance frequency of ∼100 kHz and a nominal force constant of ∼3 N/m. The AFM mica sample was prepared according to the following protocols: the hydrogel was shaken to become liquid, and 10 μL of such hydrogel solution was diluted 100 times with deionized water and dropped onto freshly cleaved mica; after 30 s of waiting time, the solution on top of the mica was rinsed off; the mica was then dried in air at 37 °C. The dried mica surface was subjected to AFM characterization. The obtained AFM images were analyzed by NT-MDT software, NOVA.

ThT Assay. The assay was performed with a Hitachi F-7000 fluorescence spectrophotometer (Tokyo, Japan). An excitation wavelength of 450 nm with a slit width of 5 nm was used. The emission spectrum in the region of 460−600 nm was measured using a slit width of 10 nm. The concentration of ThT solution was 10 μM. The PB buffer was 10 mM at pH = 7.4. The assay was performed ex situ. For each measurement, the hydrogel was shaken first to become liquid, and 10 μL of such hydrogel solution was added into 1 mL of ThT solution in a 1.0 cm quartz cuvette for fluorescence measurement.

CR Assay. The assay was performed with an Implen UV−vis nanophotometer (München, Germany). The concentration of CR solution was 5 μM. The PB buffer was 10 mM at pH = 7.4. The assay was performed ex situ. For each measurement, the hydrogel was shaken first to become liquid and 10 μL of such hydrogel solution was added into 1 mL of CR solution in a 1.0 cm quartz cuvette for UV−vis measurement.

FTIR Measurement. The FTIR measurement was performed with a Bruker Vertex 70 FTIR spectrometer (Ettlingen, Germany) equipped with a DLaTGS detector. The hydrogel was spread onto a CaF_2 window and dried in air. The CaF_2 with dried hydrogel was then subjected to FTIR measurement. The spectral acquisition parameters are: 4 cm^{-1} resolution, 32 scans, and a zero-filling factor of 2. The obtained spectrum was further smoothed with a 13-point window size using Savitzky−Golay algorithm to remove spectral noise and atmospheric water vapor interference. Smoothing was performed with Bruker OPUS software (version 7.2).

Transmission Electron Microscopy (TEM). TEM characterization was performed utilizing an FEI Tecnai G2 F20 S-TWIN transmission electron microscope (Hillsboro, Oregon) operating at 200 kV. The TEM sample was prepared according

DOI: 10.1021/acsomega.8b03492
ACS Omega 2019, 4, 8071−8080

to the following protocol. The gel sample was first diluted by 200 times with deionized water. A 200 mesh copper grid with a Formvar/carbon film was dipped into the diluted gel solution for 2 s and then put on a piece of filter paper. Ten microliters of 1% (w/v) phosphotungstic acid solution was used to stain the sample on the copper grid. The copper grid was finally air dried.

Scanning Electron Microscopy (SEM). The SEM characterization of the lyophilized hydrogel sample was performed using a JEOL JSM-7500 field emission scanning electron microscope (FE-SEM) (Tokyo, Japan) operating at 10 kV. The sample was coated with Au for observations.

X-Ray Powder Diffraction (XRD). XRD analysis was performed on a Bruker D8 advance X-ray diffractometer (Karlsruhe, Germany) using a Cu Kα radiation source. The operating conditions were λ = 1.5406 Å, voltage = 40 kV, and current = 30 mA. The lyophilized gel powder sample was loaded onto a sample plate, and the sample was analyzed for 5 h. The d-spacing were determined using Bragg's law of diffraction.

Rheological Analysis. The rheology experiment was performed by using a TA AR2000EX rheometer (New Castle, USA). The storage modulus (G′), loss modulus (G″), and the modulus of complex viscosity of the 3% (w/v) hydrogel were measured. The rheological experiments were performed at room temperature of about 20 °C in plate−plate geometry with a 20 mm plate diameter.

ANS Assay. The assay was performed with a Hitachi F-7000 fluorescence spectrophotometer (Tokyo, Japan). An excitation wavelength of 380 nm with a slit width of 5 nm was used. The emission spectrum in the region of 420−580 nm was measured using a slit width of 10 nm. The concentration of ANS solution was 20 μM. The PB buffer was 10 mM at pH = 7.4. The assay was performed ex situ. For each measurement, 2.5 μL of hydrolyzed HEWL solution was added into 1 mL of ANS solution in a 1.0 cm quartz cuvette. The solution in the cuvette was shaken first before each spectral acquisition.

Cell Cytotoxicity. Gel extract was applied to examine the cytotoxicity of the lysozyme hydrogel using L929 cell according to a published method with some modifications.[83] Briefly, 0.5 mL of hydrogel with a 30 mg/mL concentration was incubated at 37 °C in 2 mL of 1640 medium for 24 h to obtain a gel extract. L929 cells were seeded onto a 96-well plate with a suspension volume of 100 μL and a cell density of 2×10^4/mL per well. The culture medium is RPMI 1640 medium with 10% FBS. The cells were incubated at 37 °C in a balanced air humidified incubator with an atmosphere of 5% CO_2. After incubation of the cells for 24 h, the culture media were replaced by 100 μL of RPMI 1640 medium (with 10% FBS) containing gel extracts, or fresh RPMI 1640 medium (with 10% FBS) (negative control), or RPMI 1640 medium with 5% DMSO (with 10% FBS) (positive control). In addition, the extract from a commercial cell culture system, vitronectin (VTN-N), was used as an additional control. VTN-N is a recombinant human protein that provides a defined surface for the culture of human pluripotent stem cells. The cells in the above four types of culture media were allowed to be further incubated for 24 and 48 h and were then subjected to CCK-8 assay. The CCK-8 assay is an alternative cytotoxicity evaluation assay more sensitive than the common MTT assay.

■ ASSOCIATED CONTENT

Supporting Information

The Supporting Information is available free of charge on the ACS Publications website at DOI: 10.1021/acsomega.8b03492.

Maldi-TOF MS of the hydrolyzed HEWL, TEM, SEM, XRD, additional rheological tests, and UV−vis spectra of Dox and hydrolyzed HEWL (PDF)

■ AUTHOR INFORMATION

Corresponding Authors

*E-mail: haoyili.zh@gmail.com (H.L.).
*E-mail: gangma@hbu.edu.cn (G.M.).

ORCID

Gang Ma: 0000-0002-4705-145X

Author Contributions

The manuscript was written through contributions of all authors. All authors have given approval to the final version of the manuscript.

Notes

The authors declare no competing financial interest.

■ ACKNOWLEDGMENTS

We gratefully acknowledge the financial support from the National Natural Science Foundation of China (nos. 21075027 and 21773012), the Natural Science Foundation of Hebei Province (nos. B2011201082 and B2016201034), Juren plan, and Program for Changjiang Scholars and Innovative Research Team in University (no. IRT_15R16). The authors would like to thank Dr. Hongzan Song and Dr. Jianglei Qin for the helpful discussions regarding rheological analysis.

■ REFERENCES

(1) Zhang, Y. S.; Khademhosseini, A. Advances in Engineering Hydrogels. *Science* **2017**, *356*, eaaf3627.

(2) Zhu, W.; Qu, X.; Zhu, J.; Ma, X.; Patel, S.; Liu, J.; Wang, P.; Lai, C. S. E.; Gou, M.; Xu, Y.; Zhang, K.; Chen, S. Direct 3d Bioprinting of Prevascularized Tissue Constructs with Complex Microarchitecture. *Biomaterials* **2017**, *124*, 106−115.

(3) Zhao, X.; Lang, Q.; Yildirimer, L.; Lin, Z. Y.; Cui, W.; Annabi, N.; Ng, K. W.; Dokmeci, M. R.; Ghaemmaghami, A. M.; Khademhosseini, A. Photocrosslinkable Gelatin Hydrogel for Epidermal Tissue Engineering. *Adv. Healthcare Mater.* **2016**, *5*, 108−118.

(4) Taylor, D. L.; het in Panhuis, M. Self-Healing Hydrogels. *Adv. Mater.* **2016**, *28*, 9060−9093.

(5) Shao, Y.; Jia, H.; Cao, T.; Liu, D. Supramolecular Hydrogels Based on DNA Self-Assembly. *Acc. Chem. Res.* **2017**, *50*, 659−668.

(6) Mao, A. S.; Shin, J.-W.; Utech, S.; Wang, H.; Uzun, O.; Li, W.; Cooper, M.; Hu, Y.; Zhang, L.; Weitz, D. A.; Mooney, D. J. Deterministic Encapsulation of Single Cells in Thin Tunable Microgels for Niche Modelling and Therapeutic Delivery. *Nat. Mater.* **2017**, *16*, 236−243.

(7) Loessner, D.; Meinert, C.; Kaemmerer, E.; Martine, L. C.; Yue, K.; Levett, P. A.; Klein, T. J.; Melchels, F. P. W.; Khademhosseini, A.; Hutmacher, D. W. Functionalization, Preparation and Use of Cell-Laden Gelatin Methacryloyl-Based Hydrogels as Modular Tissue Culture Platforms. *Nat. Protoc.* **2016**, *11*, 727−746.

(8) Laronda, M. M.; Rutz, A. L.; Xiao, S.; Whelan, K. A.; Duncan, F. E.; Roth, E. W.; Woodruff, T. K.; Shah, R. N. A Bioprosthetic Ovary Created Using 3d Printed Microporous Scaffolds Restores Ovarian Function in Sterilized Mice. *Nat. Commun.* **2017**, *8*, 15261.

(9) Jang, J.; Park, H.-J.; Kim, S.-W.; Kim, H.; Park, J. Y.; Na, S. J.; Kim, H. J.; Park, M. N.; Choi, S. H.; Park, S. H.; Kim, S. W.; Kwon,

DOI: 10.1021/acsomega.8b03492
ACS Omega 2019, 4, 8071−8080

S.-M.; Kim, P.-J.; Cho, D.-W. 3d Printed Complex Tissue Construct Using Stem Cell-Laden Decellularized Extracellular Matrix Bioinks for Cardiac Repair. *Biomaterials* **2017**, *112*, 264−274.
(10) Grishkewich, N.; Mohammed, N.; Tang, J.; Tam, K. C. Recent Advances in the Application of Cellulose Nanocrystals. *Curr. Opin. Colloid Interface Sci.* **2017**, *29*, 32−45.
(11) Gladman, A. S.; Matsumoto, E. A.; Nuzzo, R. G.; Mahadevan, L.; Lewis, J. A. Biomimetic 4d Printing. *Nat. Mater.* **2016**, *15*, 413−418.
(12) Yesilyurt, V.; Webber, M. J.; Appel, E. A.; Godwin, C.; Langer, R.; Anderson, D. G. Injectable Self-Healing Glucose-Responsive Hydrogels with Ph-Regulated Mechanical Properties. *Adv. Mater.* **2016**, *28*, 86−91.
(13) Xing, R.; Liu, K.; Jiao, T.; Zhang, N.; Ma, K.; Zhang, R.; Zou, Q.; Ma, G.; Yan, X. An Injectable Self-Assembling Collagen-Gold Hybrid Hydrogel for Combinatorial Antitumor Photothermal/Photodynamic Therapy. *Adv. Mater.* **2016**, *28*, 3669−3676.
(14) Slaughter, B. V.; Khurshid, S. S.; Fisher, O. Z.; Khademhosseini, A.; Peppas, N. A. Hydrogels in Regenerative Medicine. *Adv. Mater.* **2009**, *21*, 3307−3329.
(15) Paul, A.; Hasan, A.; Al Kindi, H.; Gaharwar, A. K.; Rao, V. T. S.; Nikkhah, M.; Shin, S. R.; Krafft, D.; Dokmeci, M. R.; Shum-Tim, D.; Khademhosseini, A. Injectable Graphene Oxide/Hydrogel-Based Angiogenic Gene Delivery System for Vasculogenesis and Cardiac Repair. *ACS Nano* **2014**, *8*, 8050−8062.
(16) Merino, S.; Martín, C.; Kostarelos, K.; Prato, M.; Vázquez, E. Nanocomposite Hydrogels: 3d Polymer-Nanoparticle Synergies for on-Demand Drug Delivery. *ACS Nano* **2015**, *9*, 4686−4697.
(17) Dai, Y.; Ma, P.; Cheng, Z.; Kang, X.; Zhang, X.; Hou, Z.; Li, C.; Yang, D.; Zhai, X.; Lin, J. Up-Conversion Cell Imaging and Ph-Induced Thermally Controlled Drug Release from Nayf4:Yb3+/Er3+@Hydrogel Core-Shell Hybrid Microspheres. *ACS Nano* **2012**, *6*, 3327−3338.
(18) Anselmo, A. C.; Zhang, M.; Kumar, S.; Vogus, D. R.; Menegatti, S.; Helgeson, M. E.; Mitragotri, S. Elasticity of Nanoparticles Influences Their Blood Circulation, Phagocytosis, Endocytosis, and Targeting. *ACS Nano* **2015**, *9*, 3169−3177.
(19) Ma, M.; Kuang, Y.; Gao, Y.; Zhang, Y.; Gao, P.; Xu, B. Aromatic-Aromatic Interactions Induce the Self-Assembly of Pentapeptidic Derivatives in Water to Form Nanofibers and Supramolecular Hydrogels. *J. Am. Chem. Soc.* **2010**, *132*, 2719−2728.
(20) Li, J.; Zheng, C.; Cansiz, S.; Wu, C.; Xu, J.; Cui, C.; Liu, Y.; Hou, W.; Wang, Y.; Zhang, L.; Teng, I.-t.; Yang, H.-H.; Tan, W. Self-Assembly of DNA Nanohydrogels with Controllable Size and Stimuli-Responsive Property for Targeted Gene Regulation Therapy. *J. Am. Chem. Soc.* **2015**, *137*, 1412−1415.
(21) Li, J.; Kuang, Y.; Gao, Y.; Du, X.; Shi, J.; Xu, B. D-Amino Acids Boost the Selectivity and Confer Supramolecular Hydrogels of a Nonsteroidal Anti-Inflammatory Drug (Nsaid). *J. Am. Chem. Soc.* **2013**, *135*, 542−545.
(22) Komatsu, H.; Matsumoto, S.; Tamaru, S.-i.; Kaneko, K.; Ikeda, M.; Hamachi, I. Supramolecular Hydrogel Exhibiting Four Basic Logic Gate Functions to Fine-Tune Substance Release. *J. Am. Chem. Soc.* **2009**, *131*, 5580−5585.
(23) Gao, Y.; Kuang, Y.; Guo, Z.-F.; Guo, Z.; Krauss, I. J.; Xu, B. Enzyme-Instructed Molecular Self-Assembly Confers Nanofibers and a Supramolecular Hydrogel of Taxol Derivative. *J. Am. Chem. Soc.* **2009**, *131*, 13576−13577.
(24) Appel, E. A.; Biedermann, F.; Rauwald, U.; Jones, S. T.; Zayed, J. M.; Scherman, O. A. Supramolecular Cross-Linked Networks Via Host-Guest Complexation with Cucurbit 8 Uril. *J. Am. Chem. Soc.* **2010**, *132*, 14251−14260.
(25) Kabanov, A. V.; Vinogradov, S. V. Nanogels as Pharmaceutical Carriers: Finite Networks of Infinite Capabilities. *Angew. Chem. Int. Ed.* **2009**, *48*, 5418−5429.
(26) Zhang, L.; Cao, Z.; Bai, T.; Carr, L.; Ella-Menye, J.-R.; Irvin, C.; Ratner, B. D.; Jiang, S. Zwitterionic Hydrogels Implanted in Mice Resist the Foreign-Body Reaction. *Nat. Biotechnol.* **2013**, *31*, 553−556.
(27) Li, P.; Poon, Y. F.; Li, W.; Zhu, H.-Y.; Yeap, S. H.; Cao, Y.; Qi, X.; Zhou, C.; Lamrani, M.; Beuerman, R. W.; Kang, E.-T.; Mu, Y.; Li, C. M.; Chang, M. W.; Leong, S. S. J.; Chan-Park, M. B. A Polycationic Antimicrobial and Biocompatible Hydrogel with Microbe Membrane Suctioning Ability. *Nat. Mater.* **2011**, *10*, 149−156.
(28) Agarwal, R.; García, A. J. Biomaterial Strategies for Engineering Implants for Enhanced Osseointegration and Bone Repair. *Adv. Drug Deliv.Rev.* **2015**, *94*, 53−62.
(29) Pinkas, O.; Goder, D.; Noyvirt, R.; Peleg, S.; Kahlon, M.; Zilberman, M. Structuring of Composite Hydrogel Bioadhesives and Its Effect on Properties and Bonding Mechanism. *Acta Biomater.* **2017**, *51*, 125−137.
(30) Bhagat, V.; Becker, M. L. Degradable Adhesives for Surgery and Tissue Engineering. *Biomacromolecules* **2017**, *18*, 3009−3039.
(31) Balcioglu, S.; Parlakpinar, H.; Vardi, N.; Denkbas, E. B.; Karaaslan, M. G.; Gulgen, S.; Taslidere, E.; Koytepe, S.; Ates, B. Design of Xylose-Based Semisynthetic Polyurethane Tissue Adhesives with Enhanced Bioactivity Properties. *ACS Appl. Mater. Interfaces* **2016**, *8*, 4456−4466.
(32) Han, L.; Lu, X.; Liu, K.; Wang, K.; Fang, L.; Weng, L.-T.; Zhang, H.; Tang, Y.; Ren, F.; Zhao, C.; Sun, G.; Liang, R.; Li, Z. Mussel-Inspired Adhesive and Tough Hydrogel Based on Nanoclay Confined Dopamine Polymerization. *ACS Nano* **2017**, *11*, 2561−2574.
(33) Yu, L.; Ding, J. Injectable Hydrogels as Unique Biomedical Materials. *Chem. Soc. Rev.* **2008**, *37*, 1473−1481.
(34) Guvendiren, M.; Lu, H. D.; Burdick, J. A. Shear-Thinning Hydrogels for Biomedical Applications. *Soft Matter* **2012**, *8*, 260−272.
(35) Xing, R.; Li, S.; Zhang, N.; Shen, G.; Möhwald, H.; Yan, X. Self-Assembled Injectable Peptide Hydrogels Capable of Triggering Antitumor Immune Response. *Biomacromolecules* **2017**, *18*, 3514−3523.
(36) Phipps, M. C.; Monte, F.; Mehta, M.; Kim, H. K. W. Intraosseous Delivery of Bone Morphogenic Protein-2 Using a Self-Assembling Peptide Hydrogel. *Biomacromolecules* **2016**, *17*, 2329−2336.
(37) Oyen, E.; Martin, C.; Caveliers, V.; Madder, A.; Van Mele, B.; Hoogenboom, R.; Hernot, S.; Ballet, S. In Vivo Imaging of the Stability and Sustained Cargo Release of an Injectable Amphipathic Peptide-Based Hydrogel. *Biomacromolecules* **2017**, *18*, 994−1001.
(38) Nandi, N.; Gayen, K.; Ghosh, S.; Bhunia, D.; Kirkham, S.; Sen, S. K.; Ghosh, S.; Hamley, I. W.; Banerjee, A. Amphiphilic Peptide-Based Supramolecular, Noncytotoxic, Stimuli-Responsive Hydrogels with Antibacterial Activity. *Biomacromolecules* **2017**, *18*, 3621−3629.
(39) Lindsey, S.; Piatt, J. H.; Worthington, P.; Sönmez, C.; Satheye, S.; Schneider, J. P.; Pochan, D. J.; Langhans, S. A. Beta Hairpin Peptide Hydrogels as an Injectable Solid Vehicle for Neurotrophic Growth Factor Delivery. *Biomacromolecules* **2015**, *16*, 2672−2683.
(40) Fan, Z.; Fu, M.; Xu, Z.; Zhang, B.; Li, Z.; Li, H.; Zhou, X.; Liu, X.; Duan, Y.; Lin, P.-H.; Duann, P.; Xie, X.; Ma, J.; Liu, Z.; Guan, J. Sustained Release of a Peptide-Based Matrix Metalloproteinase-2 Inhibitor to Attenuate Adverse Cardiac Remodeling and Improve Cardiac Function Following Myocardial Infarction. *Biomacromolecules* **2017**, *18*, 2820−2829.
(41) Baral, A.; Roy, S.; Ghosh, S.; Hermida-Merino, D.; Hamley, I. W.; Banerjee, A. A Peptide-Based Mechano-Sensitive, Proteolytically Stable Hydrogel with Remarkable Antibacterial Properties. *Langmuir* **2016**, *32*, 1836−1845.
(42) Baral, A.; Roy, S.; Dehsorkhi, A.; Hamley, I. W.; Mohapatra, S.; Ghosh, S.; Banerjee, A. Assembly of an Injectable Noncytotoxic Peptide-Based Hydrogelator for Sustained Release of Drugs. *Langmuir* **2014**, *30*, 929−936.
(43) Mano, J. F. Stimuli-Responsive Polymeric Systems for Biomedical Applications. *Adv. Eng. Mater.* **2008**, *10*, 515−527.
(44) Li, Y.; Rodrigues, J.; Tomás, H. Injectable and Biodegradable Hydrogels: Gelation, Biodegradation and Biomedical Applications. *Chem. Soc. Rev.* **2012**, *41*, 2193−2221.
(45) Koutsopoulos, S.; Unsworth, L. D.; Nagai, Y.; Zhang, S. Controlled Release of Functional Proteins through Designer Self-

DOI: 10.1021/acsomega.8b03492
ACS Omega 2019, 4, 8071−8080

Assembling Peptide Nanofiber Hydrogel Scaffold. *Proc. Natl. Acad. Sci. U. S. A.* **2009**, *106*, 4623−4628.
(46) Altunbas, A.; Lee, S. J.; Rajasekaran, S. A.; Schneider, J. P.; Pochan, D. J. Encapsulation of Curcumin in Self-Assembling Peptide Hydrogels as Injectable Drug Delivery Vehicles. *Biomaterials* **2011**, *32*, 5906−5914.
(47) Thota, C. K.; Yadav, N.; Chauhan, V. S. A Novel Highly Stable and Injectable Hydrogel Based on a Conformationally Restricted Ultrashort Peptide. *Sci. Rep.* **2016**, *6*, 31167.
(48) Mahler, A.; Reches, M.; Rechter, M.; Cohen, S.; Gazit, E. Rigid, Self-Assembled Hydrogel Composed of a Modified Aromatic Dipeptide. *Adv. Mater.* **2006**, *18*, 1365−1370.
(49) Loo, Y.; Zhang, S.; Hauser, C. A. E. From Short Peptides to Nanofibers to Macromolecular Assemblies in Biomedicine. *Biotechnol. Adv.* **2012**, *30*, 593−603.
(50) Nanda, J.; Biswas, A.; Banerjee, A. Single Amino Acid Based Thixotropic Hydrogel Formation and Ph-Dependent Morphological Change of Gel Nanofibers. *Soft Matter* **2013**, *9*, 4198−4208.
(51) Fichman, G.; Gazit, E. Self-Assembly of Short Peptides to Form Hydrogels: Design of Building Blocks, Physical Properties and Technological Applications. *Acta Biomater.* **2014**, *10*, 1671−1682.
(52) Basu, K.; Baral, A.; Basak, S.; Dehsorkhi, A.; Nanda, J.; Bhunia, D.; Ghosh, S.; Castelletto, V.; Hamley, I. W.; Banerjee, A. Peptide Based Hydrogels for Cancer Drug Release: Modulation of Stiffness, Drug Release and Proteolytic Stability of Hydrogels by Incorporating D-Amino Acid Residue(S). *Chem. Commun.* **2016**, *52*, 5045−5048.
(53) Eskandari, S.; Guerin, T.; Toth, I.; Stephenson, R. J. Recent Advances in Self-Assembled Peptides: Implications for Targeted Drug Delivery and Vaccine Engineering. *Adv. Drug Delivery Rev.* **2017**, *110*, 169−187.
(54) Chiti, F.; Dobson, C. M. Protein Misfolding, Functional Amyloid, and Human Disease. *Annu. Rev. Biochem.* **2006**, *75*, 333−366.
(55) Sawaya, M. R.; Sambashivan, S.; Nelson, R.; Ivanova, M. I.; Sievers, S. A.; Apostol, M. I.; Thompson, M. J.; Balbirnie, M.; Wiltzius, J. J. W.; McFarlane, H. T.; Madsen, A. Ø.; Riekel, C.; Eisenberg, D. Atomic Structures of Amyloid Cross-Beta Spines Reveal Varied Steric Zippers. *Nature* **2007**, *447*, 453−457.
(56) Semerdzhiev, S. A.; Dekker, D. R.; Subramaniam, V.; Claessens, M. M. A. E. Self-Assembly of Protein Fibrils into Suprafibrillar Aggregates: Bridging the Nano- and Mesoscale. *ACS Nano* **2014**, *8*, 5543−5551.
(57) Bhak, G.; Lee, S.; Park, J. W.; Cho, S.; Paik, S. R. Amyloid Hydrogel Derived from Curly Protein Fibrils of Alpha-Synuclein. *Biomaterials* **2010**, *31*, 5986−5995.
(58) Zhou, X.-M.; Shimanovich, U.; Herling, T. W.; Wu, S.; Dobson, C. M.; Knowles, T. P. J.; Perrett, S. Enzymatically Active Microgels from Self-Assembling Protein Nanofibrils for Microflow Chemistry. *ACS Nano* **2015**, *9*, 5772−5781.
(59) Hauser, C. A. E.; Maurer-Stroh, S.; Martins, I. C. Amyloid-Based Nanosensors and Nanodevices. *Chem. Soc. Rev.* **2014**, *43*, 5326−5345.
(60) Knowles, T. P. J.; Mezzenga, R. Amyloid Fibrils as Building Blocks for Natural and Artificial Functional Materials. *Adv. Mater.* **2016**, *28*, 6546−6561.
(61) Li, C.; Adamcik, J.; Mezzenga, R. Biodegradable Nanocomposites of Amyloid Fibrils and Graphene with Shape-Memory and Enzyme-Sensing Properties. *Nat. Nanotechnol.* **2012**, *7*, 421−427.
(62) Reynolds, N. P.; Charnley, M.; Mezzenga, R.; Hartley, P. G. Engineered Lysozyme Amyloid Fibril Networks Support Cellular Growth and Spreading. *Biomacromolecules* **2014**, *15*, 599−608.
(63) Shimanovich, U.; Efimov, I.; Mason, T. O.; Flagmeier, P.; Buell, A. K.; Gedanken, A.; Linse, S.; Åkerfeldt, K. S.; Dobson, C. M.; Weitz, D. A.; Knowles, T. P. J. Protein Microgels from Amyloid Fibril Networks. *ACS Nano* **2015**, *9*, 43−51.
(64) Wei, G.; Su, Z.; Reynolds, N. P.; Arosio, P.; Hamley, I. W.; Gazit, E.; Mezzenga, R. Self-Assembling Peptide and Protein Amyloids: From Structure to Tailored Function in Nanotechnology. *Chem. Soc. Rev.* **2017**, *46*, 4661−4708.
(65) Zou, Y.; Li, Y.; Hao, W.; Hu, X.; Ma, G. Parallel β-Sheet Fibril and Antiparallel β-Sheet Oligomer: New Insights into Amyloid Formation of Hen Egg White Lysozyme under Heat and Acidic Condition from FTIR Spectroscopy. *J. Phys. Chem. B* **2013**, *117*, 4003−4013.
(66) Zou, Y.; Hao, W.; Li, H.; Gao, Y.; Sun, Y.; Ma, G. New Insight into Amyloid Fibril Formation of Hen Egg White Lysozyme Using a Two-Step Temperature-Dependent Ftir Approach. *J. Phys. Chem. B* **2014**, *118*, 9834−9843.
(67) Qin, Z.; Sun, Y.; Jia, B.; Wang, D.; Ma, Y.; Ma, G. Kinetic Mechanism of Thioflavin T Binding onto the Amyloid Fibril of Hen Egg White Lysozyme. *Langmuir* **2017**, *33*, 5398−5405.
(68) Proctor, V. A.; Cunningham, F. E.; Fung, D. Y. C. The Chemistry of Lysozyme and Its Use as a Food Preservative and a Pharmaceutical. *Crit. Rev. Food Sci. Nutr.* **1988**, *26*, 359−395.
(69) Smith, B. J. In *The Protein Protocols Handbook*; Walker, J. M., Ed.; Humana Press: Totowa, New Jersey, 2002; p 499−502.
(70) Frare, E.; de Laureto, P. P.; Zurdo, J.; Dobson, C. M.; Fontana, A. A Highly Amyloidogenic Region of Hen Lysozyme. *J. Mol. Biol.* **2004**, *340*, 1153−1165.
(71) Mishra, R.; Sörgjerd, K.; Nyström, S.; Nordigården, A.; Yu, Y.-C.; Hammarström, P. Lysozyme Amyloidogenesis Is Accelerated by Specific Nicking and Fragmentation but Decelerated by Intact Protein Binding and Conversion. *J. Mol. Biol.* **2007**, *366*, 1029−1044.
(72) LeVine, H., III [18] Quantification of β-sheet Amyloid Fibril Structures with Thioflavin T. *Methods Enzymol.* **1999**, *309*, 274−284.
(73) Klunk, W. E.; Jacob, R. F.; Mason, R. P. [19] Quantifying Amyloid by Congo Red Spectral Shift Assay. *Methods Enzymol.* **1999**, *309*, 285−305.
(74) Barth, A.; Zscherp, C. What Vibrations Tell Us About Proteins. *Q. Rev. Biophys.* **2002**, *35*, 369−430.
(75) Jiang, L.; Xu, D.; Sellati, T. J.; Dong, H. Self-Assembly of Cationic Multidomain Peptide Hydrogels: Supramolecular Nanostructure and Rheological Properties Dictate Antimicrobial Activity. *Nanoscale* **2015**, *7*, 19160−19169.
(76) Motamed, S.; Del Borgo, M. P.; Kulkarni, K.; Habila, N.; Zhou, K.; Perlmutter, P.; Forsythe, J. S.; Aguilar, M. I. A Self-Assembling β-peptide Hydrogel for Neural Tissue Engineering. *Soft Matter* **2016**, *12*, 2243−2246.
(77) Stryer, L. The Interaction of a Naphthalene Dye with Apomyoglobin and Apohemoglobin. A Fluorescent Probe of Non-Polar Binding Sites. *J. Mol. Biol.* **1965**, *13*, 482−495.
(78) Hawe, A.; Sutter, M.; Jiskoot, W. Extrinsic Fluorescent Dyes as Tools for Protein Characterization. *Pharm. Res.* **2008**, *25*, 1487−1499.
(79) Wang, J.; Liu, K.; Xing, R.; Yan, X. Peptide Self-Assembly: Thermodynamics and Kinetics. *Chem. Soc. Rev.* **2016**, *45*, 5589−5604.
(80) Xing, R.; Yuan, C.; Li, S.; Song, J.; Li, J.; Yan, X. Charge-Induced Secondary Structure Transformation of Amyloid-Derived Dipeptide Assemblies from β-Sheet to α-Helix. *Angew. Chem.Int. Ed.* **2018**, *57*, 1537−1542.
(81) Soto, C. Unfolding the Role of Protein Misfolding in Neurodegenerative Diseases. *Nat Rev Neurosci* **2003**, *4*, 49−60.
(82) Gao, Y.; Zou, Y.; Ma, Y.; Wang, D.; Sun, Y.; Ma, G. Infrared Probe Technique Reveals a Millipede-Like Structure for Aβ(8−28) Amyloid Fibril. *Langmuir* **2016**, *32*, 937−946.
(83) Chen, Y.; Wang, W.; Wu, D.; Nagao, M.; Hall, D. G.; Thundat, T.; Narain, R. Injectable Self-Healing Zwitterionic Hydrogels Based on Dynamic Benzoxaborole-Sugar Interactions with Tunable Mechanical Properties. *Biomacromolecules* **2018**, *19*, 596−605.

DOI: 10.1021/acsomega.8b03492
ACS Omega 2019, 4, 8071−8080